2-Aryl-1,3,4-trifluoro-6,7,10,11-tetrakis(alkoxy)triphenylene: a remarkable and highly inclusive mesomorphic platform

Hui-Min Pan, Jiao He, Wen-Hao Yu, Ping Hu, Bi-Qin Wang, Ke-Qing Zhao, Bertrand Donnio

2-Aryl-1,3,4-trifluoro-6,7,10,11-tetrakis(alkoxy)triphenylene: a remarkable and highly inclusive mesomorphic platform †

Hui-Min Pan,[a] Jiao He,[a] Wen-Hao Hu,[a] Ping Hu,[a] Bi-Qin Wang,[a] Ke-Qing Zhao,*[a] and Bertrand Donnio*[b]

[a] College of Chemistry and Materials Science, Sichuan Normal University, Chengdu 610066, China. E-mail: kqzhao@sicnu.edu.cn
[b] Institut de Physique et Chimie des Matériaux de Strasbourg (IPCMS), UMR7504, CNRS-Université de Strasbourg, Strasbourg 67034, France. E-mail: bertrand.donnio@ipcms.unistra.fr

Cite as : J. Mater. Chem. C **2023**, *11*, 14965-14704 (DOI: 10.1039/d3tc02569a).

† Electronic supplementary information (ESI) available. See DOI: https://doi.org/10.1039/d3tc02569a
Crystal structure data https://www.rsc.org/suppdata/d3/tc/d3tc02569a/d3tc02569a2.cif

Manuscript received: July 20, 2023
Accepted manuscript online: September 26, 2023
Version of record online: September 27, 2023

Non-covalent Q4arene–fluoroarene interactions have been increasingly exploited to create complex, soft and/or rigid supramolecular assemblies and more recently to design liquid crystals.

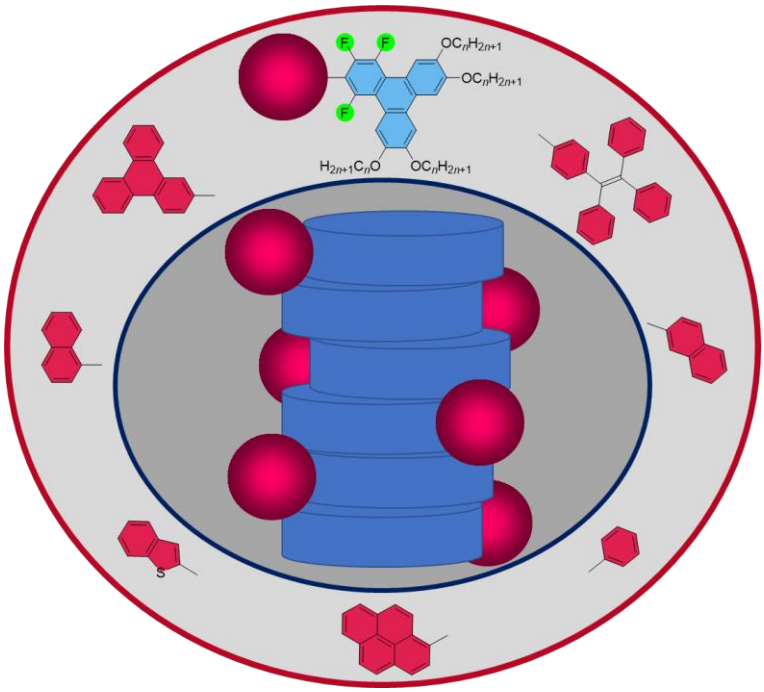

Abstract Non-covalent arene-fluoroarene interactions are increasingly exploited to create complex, soft and/or rigid supramolecular assemblies and more recently to design liquid crystals. These interactions stem from the strong electronegativity of the fluorine atoms which modifies the dipole moment of the fluorinated aromatic rings. Here, two new series of fluorine-containing triphenylene derivatives bearing 4 peripheral alkyl chains of various lengths were synthesized by nucleophilic substitution of fluoroarenes (S_NFAr). A first monotonous series i.e. 2-phenyl-1,3,4-trifluorotriphenylenes (**PH***n*, R = C_nH_{2n+1}, *n* = 3-12) was obtained in ca. 60-90% yields by reacting lipophilic 2,2'-dilithiobiphenyl derivatives with pentafluorobiphenyl C_6F_5-C_6H_5. Following a similar synthetic procedure, a second series of analogous compounds with larger functional aryl pending moieties, i.e. 2-aryl-1,3,4-trifluorotriphenylene derivatives, such as naphthalen-1/2-yl (**NAA**/**NAB**), benzothiophen-2-yl (**BT**), triphenylen-2-yl (**TP**), pyren-1-yl (**PY**) and tetraphenylethylenyl (**TPE**), was also prepared and obtained in moderate to high yields. Quite remarkably, induction and/or stabilization of columnar mesophases were systematically observed for all these new fluorine-containing triphenylene derivatives. **PH***n* show wide ranges of Col_{hex} phases including room temperature with clearing temperatures that gradually decrease with the lengthening of the alkyl chains, in contrast to the analogous non-fluorinated triphenylene derivative deprived of liquid crystal properties. **BT**8, **NAA**8, **NAB**8, **TP**8, **PY**8, **TPE**8, consistently display a columnar hexagonal (Col_{hex}) mesophase whilst their mesophase ranges, though also broad, depend strongly on the size and bulkiness of the side aromatic residue. This study demonstrates the essential role played by aromatic fluorination and the predominance of arene-fluoroarene supramolecular interactions in the effective induction of mesophases by directing face-to-face stacking of aromatic rings of opposite nature. An X-ray single-crystal structure of **PH**0 indeed reveals the presence of such arene-fluoarene interactions in the solid state and the antiparallel π-π stacking pattern. All the fluorinated molecules show blue photoluminescence in diluted solution, with fluorescent absolute quantum yield as high as 57% for the **PY**-containing triphenylene. **PY**8 reveals high hole transport mobility rate in the range of 10^{-3} cm^2 V^{-1} s^{-1} as measured by TOF, in similar range than other triphenylene-containing homologs.

Introduction

Discotic liquid crystals (DLCs)[1-6] are unique type of soft supramolecular functional materials with dynamic and order degree features, and have been widely studied for their great potential commercial applications in the liquid crystal display industry,[7] as well as in organic electronics,[8-12] magnetic[13] and optical advanced materials.[6,7] DLCs usually consist of a polycyclic aromatic core and several peripheral alkoxy chains,[1] and they are essentially electron-rich π-systems. The synthesis of most polycyclic aromatic discogens is mainly based on transition metal catalyzed-based reactions such as Suzuki-Miyaura, Heck, Sonogashira cross-couplings and oxidative π-extended Scholl reactions.[14-19] Triphenylene derivatives are overwhelming in DLCs,[20] and the archetypical representative, i.e. 2,3,6,7,10,11-hexakis(alkoxy)triphenylenes, can be simply prepared in large scale in one step by the highly efficient oxidative trimerization of 1,2-dialkoxybenzene catalyzed by $FeCl_3$ in MeOH.[21] Triphenylene-based DLCs play an important role in the design of many new functional materials, so the development of practical and efficient, and preferably without the use of noble transition metal-based catalysts (i.e. Ag, Au, Ni, Pd, Pt, Rh, Ir, Ru, …), synthetic methodologies continues to attract organic and materials chemists to expand the type of functionalities and but also to increase the structural diversity of this ubiquitous molecular system.[22-24]

Fluorine atom is small but possesses a strong electron-withdrawing ability due to its strong electronegativity. Substitution of aromatic cores by fluorine atoms thus changes drastically the electronic properties of the π-conjugating systems and will affect their supramolecular architectures and organizations.[25-28] The synthesis of fluorine-substituted DLCs begins to spark the interest of materials' chemists,[29-37] as in addition to bring novelty, non-covalent arene-perfluoroarene intermolecular interactions may emerge, which strongly favor induction and/or stabilization of columnar mesophases by supramolecular stacking.[38] It also represents an elegant way to produce novel DLC systems.[38,39] However, few syntheses of fluorine-containing DLCs have been reported up to now, so reliable, economical and environmentally friendly synthetic methods are absolutely essential.

We recently reported an effective synthetic methodology based on the nucleophilic substitution of fluoroarene (S_NFAr) to produce a wide range of original fluorine-containing DLCs.[40] Here, we propose an extension of this chemistry to synthesize aryl-functionalized fluorine triphenylene derivatives. The "fluorine-substituted triphenylene" motif with only four alkoxy chains was found to be a remarkable and inclusive

mesogenic promoter as columnar mesophases were systematically formed even after the connection of large bulky functional aromatic fragments, such as benzothiophene (**BT**), naphthalene (**NAA** and **NAB**), pyrene (**PY**), triphenylene (**TP**) and tetraphenylethene (**TPE**). The photophysical and semiconducting properties, as well as the self-organizing mesomorphism of these systems are reported and discussed with respect to chain-lengths and side-groups.

Results and Discussion

Synthetic procedures

A very efficient synthetic strategy based on the nucleophilic substitution of fluoroarene was applied for the preparation of these new families of fluorinated discotic compounds (Scheme 1). Both biphenylene precursors, i.e. 2,3,4,5,6-pentafluoro-1,1'-biphenyl (Scheme S1, C_6H_5-C_6F_5) and 2,2'-dibromo-4,4',5,5'-tetrakis(alkoxy)-1,1'-biphenyl (Schemes 1 and S2, 2Br-**BP***n*) building blocks, were prepared with high selectivity and in good yields (85% and 60-79%, respectively) by the direct nucleophilic mono-substitution reaction between phenyllithium (obtained *in situ* from bromobenzene) and hexafluorobenzene[26,27] or by the $FeCl_3$-catalyzed Scholl reaction from 1-bromo-3,4-bis(alkoxy)benzene,[41] respectively. Reaction of 2Br-**BP***n* with *n*-butyllithium yielded quantitatively 2,2'-dilithiobiphenyls (2Li-**BP***n*), which then underwent *in situ* aryl nucleophilic substitution (S_NAr) reaction with C_6F_5-C_6H_5 to give the target compounds, 2-phenyl-1,3,4-trifluoro-6,7,10,11-tetrakis(alkoxy)triphenylene (Scheme 1, **PH***n*, *n* = 3-12) in yields ranging between 61 to 87% (Scheme 1).

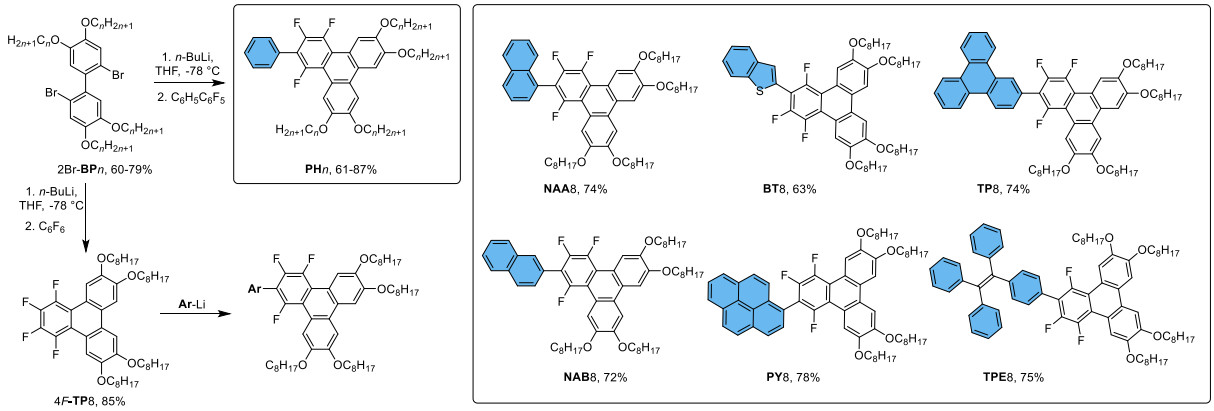

Scheme 1. Synthesis, Molecular Structures, Nomenclature and Yields of the 2-aryl-1,3,4-trifluorotriphenylenes.

Applying the above reaction conditions, 2-phenyl-1,3,4-trifluorotriphenylene (**PH**0), i.e. with no alkoxy chain, was prepared in 42% yields (Scheme S3) for single crystal growth and molecular structure analysis, and to confirm the annulation reaction pattern. For direct comparison of the impact of fluorine atom on the mesomorphism and the role of arene-fluoroarene interactions on mesophase stabilization, a non-fluorine homolog, namely 2,3,6,7-tetrakis(hexyloxy)-10-phenyltriphenylene (**BTP**6), was also synthesized by the Pd-catalyzed Suzuki-Miyaura cross-coupling and $FeCl_3$ Scholl intramolecular oxidative cyclization reactions' tandem (Schemes S4).[14-19]

Prior to the preparation of the functional set of aryl-substituted triphenylene derivatives, 2Li-**BP**8 was first reacted with C_6F_6 to yield 1,2,3,4-tetrafluorotriphenylene (4*F*-**TP**8, Scheme S5).[40] Once isolated, 4*F*-**TP**8 was further reacted with the various **Ar**-Li, prepared *in situ* beforehand by reacting the various arylbromides (**Ar**-Br) with *n*-butyllithium, to produce the target fluorinated derivatives, abbreviated as **BT**8, **NAA**8, **NAB**8, **PY**8, **TP**8 and **TPE**8 (Scheme 1).

This S_NFAr synthetic method is thus facile, efficient, and highly reliable and last but not least, does not require any precious transition metal as catalyst (transition metal-free) of interest for gram-scale production of fluorous discotic structures. The structure and purity of all the compounds were confirmed by $^1H/^{13}C/^{19}F$ NMR (Figure S1-S54), elemental analysis and high-resolution mass spectrometry (HRMS, Figure S55-S68).

Crystal structure

Single crystals of **PH**0 suitable for X-ray analysis were obtained by slow evaporation of ethyl acetate solution, and the results are displayed in Figure 1 and additional information is reported in Tables S1-6. The crystal unit cell is monoclinic with the $P2_1/n$ space group (no. 14). The crystal unit cell [a = 13.2645(2) Å, b = 5.5284(1) Å, c = 22.7571(3) Å, β = 102.651(1) °, V = 1628.30(4) $Å^3$] contains 4 molecules, which gives a calculated density of 1.462 g/cm^3. The crystal structure is a direct and unequivocal proof that the S_NFAr reaction of 2,2'-dilithio-1,1'-biphenyl with 2,3,4,5,6-pentafluoro-1,1'-biphenyl yields 1,2,4-trifluoro-3-phenyltriphenylene worked and occurred at the expected positions. The ^{19}F-NMR spectra of **PH**0 and of the alkoxy-substituted substrates **PH***n* show 3 single peaks at almost identical positions (Figures S31-S37), which confirms that the substitution pattern is the same for all these triphenylene derivatives. Furthermore, it also reveals the high planarity of the fluoro-containing triphenylene core, with, however, a substantial planar deviation of the pending phenyl group forming a large tilt of ca. 70° with the triphenylene (Figure S70a). This compound can pile on top of each other by optimizing arene-fluoroarene interactions between fluorine-containing and fluorine-free zones of the central triphenylene fragment, indeed possible due to the absence of aliphatic chains. The crystal structure shows numerous F−H intermolecular short contacts of ca. 2.58-2.67 Å and larger distances of 4.34 and 5.53 Å between centroids of the closest stacked molecules (Figure S70b), which are responsible to this highly coplanar but slightly offset stack.[29]

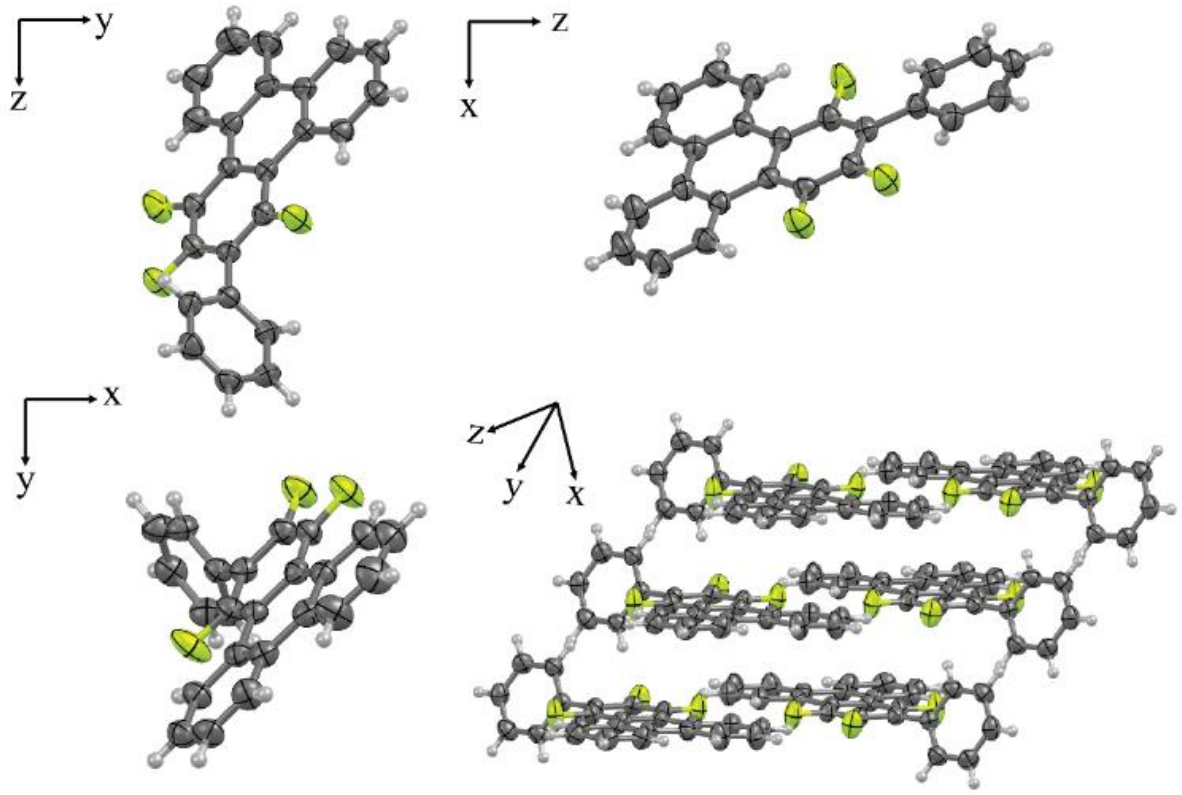

Figure 1. Molecular structure of 1,2,4-trifluoro-3-phenyltriphenylene, **PH**0, and anti-parallel and shifted stacking of the flat cores in the crystalline phase.

Thermal stability and mesomorphic properties

The thermal stability of these functional fluorinated organic materials, crucial for the applications' processing and physical properties studies, was investigated by thermogravimetric analysis (TGA, Figure S71) in dynamic mode (scan rate of 10 °C/min). The results showed that all **PH***n* have very good thermal stability, with decomposition temperatures at 5% weight loss all above 310 °C; **PH**8, with 4 C_8H_{17} chains, possesses the highest decomposition temperature (354 °C), and thus the highest thermal stability. The presence and the nature of various aryl pending groups do not affect significantly the overall thermal stability, as also, all six 2-aryl-1,3,4-trifluorotriphenylene compounds (**BT**8, **NAA**8, **NAB**8, **PY**8, **TP**8, **TPE**8, Scheme 1) display slightly

higher decomposition temperatures, above 345 °C (as determined at the 5% weight loss) than **PH***n* compounds; for information, the tetrafluorotriphenylene precursor, 4*F*-**TP**8, decomposes at ca 300 °C.[40] In all cases, the investigation of the mesophase was performed well below those temperatures.

The thermotropic liquid crystalline properties of the synthesized molecules were studied by polarizing optical microscopy (POM, Figure 2 and S72) and differential scanning calorimetry (DSC, Figures S73 and S74, Table S7). All the phenyl-substituted triphenylenes **PH***n* display optical textures with typical linear defects or fan-shaped optical textures as well as large homeotropic domains (Figure 2a as a typical example), characteristic of a columnar hexagonal mesophase, Col_{hex}.

For the shorter terms **PH**3/4/6, another phase could be detected at lower temperatures by DSC only (still with hexagonal symmetry as revealed by S/WAXS, and no detectable changes in the POM texture, vide supra). Furthermore, **PH**3 behaves also quite differently, in that a crystallization event is observed on second heating at around 100 °C (cold crystallization). No crystallization is observed for compounds **PH**6/8, whereas the longer chains' homologs, **PH**10/12, crystallize around zero Celsius. In this series, the clearing temperatures decrease upon alkyl chain lengthening (Figure 3a). For comparison, the fully hydrogenated molecular homolog, **BTP**6 (Figure 3a), is not mesomorphous, which clearly demonstrates the importance of the fluorine aromatic substitution in the induction of columnar mesophases with high stability, indebted to the establishment of effective arene-fluoroarene interactions.

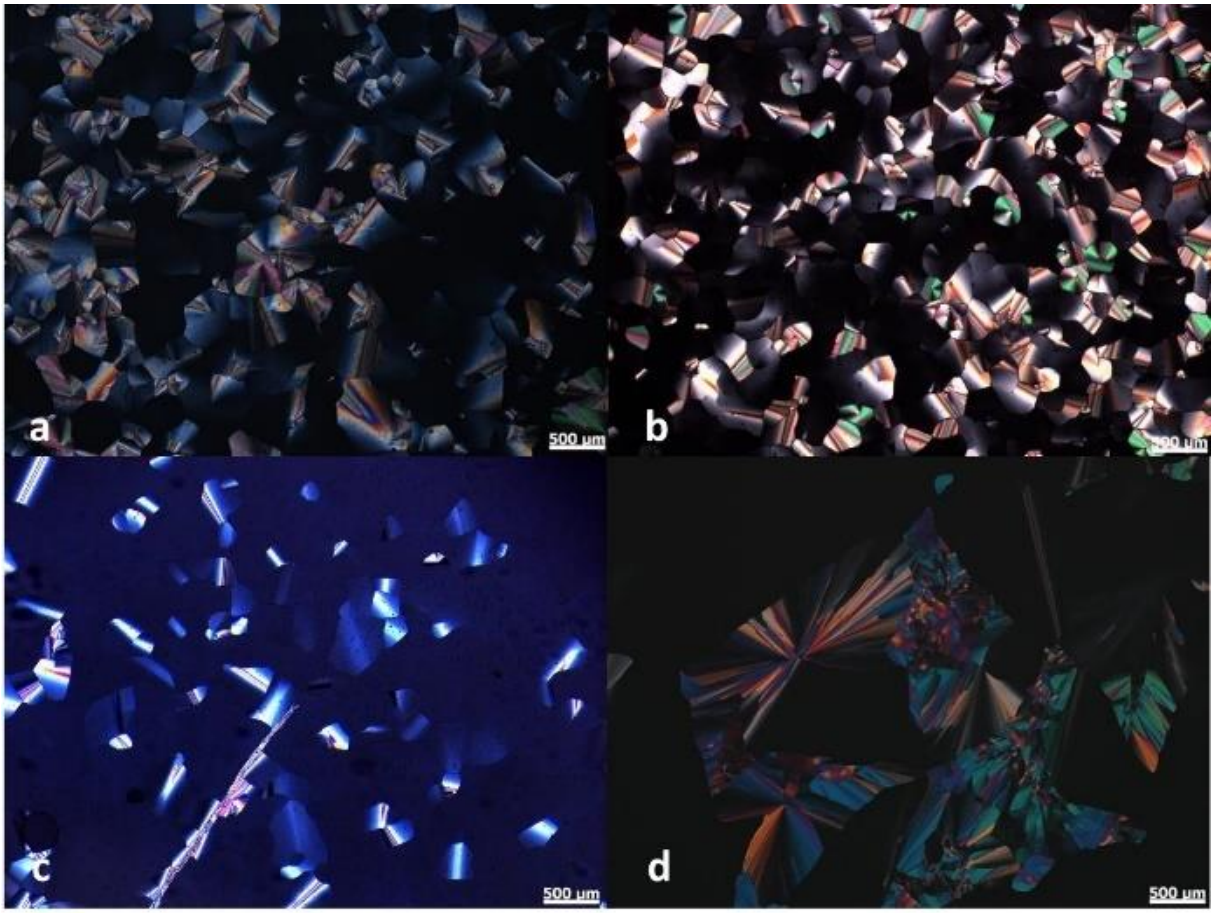

Figure 2. Representative POM textures of some of the fluorinated mesogens: a) **PH**8, 111 °C, b) **NAA**8, 45 °C, c) **NAB**8, 162 °C, d) **TPE**8, 95 °C (Images taken on slow cooling from isotropic liquid at a rate of 2 °C/min; scale bar represents 500 µm for all).

Similarly, the other six substituted triphenylene molecules with larger pending aromatic fragments all exhibit a columnar mesophase as deduced from POM and DSC, despite the bulkiness of the aryl moieties. The POM observation of highly fluid textures with fan-shaped features and large homeotropic zones (Figure 2b-d) suggests that a Col_{hex} phase is also induced in these systems. The less bulky molecule, **BT**8, excluding momentarily **PH**8, exhibits the highest clearing temperature and is crystalline up to ca. 100 °C, whilst all the

other compounds show room temperature columnar mesophases, with the clearing temperatures depending of the aryl nature (Figure 3b). Mesogens with pyren-1-yl fragments (**PY**) and naphthalen-1-yl (**NAA**) and that with the bulkier tetraphenylethylenyl (**TPE**) side-groups, show the lowest clearing temperatures of this set of compounds. This reduction of the mesophase stability can be explained by the out-of-plane torsion of the appended pyrene and naphthalene fragments with respect to the triphenylene plane (in **PY**8 and **NAA**8, respectively) and by the free-rotation of the four phenyl rings of **TPE**8 (DFT, Tables S11-S12), that probably perturb the regular π-π stacking and strongly reduce the arene-fluoroarene overlaps, thus resulting in the overall weakening of the intermolecular interactions. In contrast, for **BT**8 and **NAB**8 mesogens, both benzothiophen-2-yl (**BT**) and naphthalen-2-yl (**NAB**) fragments can rotate around the bond connecting with the triphenylene moiety, as the phenyl group in **PH***n*, without greatly perturbing the columnar stacking and intermolecular interactions, hence the higher mesophase stability. The behavior of **TP**8 appears counter-intuitive at first but even with strong deviation from the plane, the overlap between fluoro-containing and fluoro-free zones of the central triphenylene fragment can nevertheless be optimized via face-to-face stacking with a head-to-head arrangement resulting in the formation of columns. These results show that the fluorine substituted triphenylene with four octyloxy chains can accommodate bulky aryl groups within columnar stacking, with a very high ability to promote piling and to stabilize columnar mesophase.

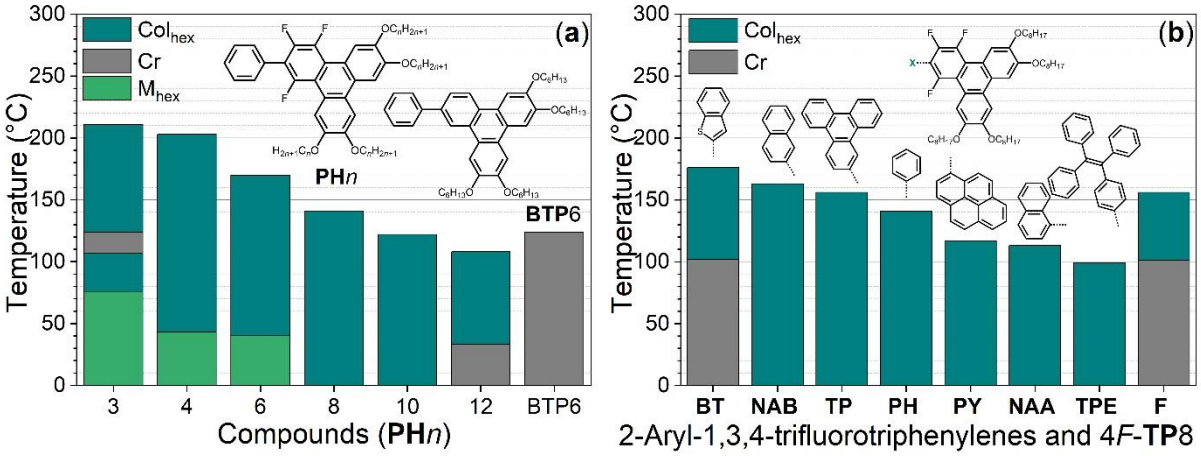

Figure 3. Phase diagram of (a) **PH***n* (compared with **BTP**6) and (b) 2-aryl-1,3,4-trifluorotriphenylenes (compared with 4*F*-**TP**8[40]).

Temperature-dependent X-ray scattering experiments were systematically carried out on all compounds in order to unequivocally identify the nature of the mesophase. The X-ray patterns were recorded at several temperatures between room temperature and the isotropic liquid (Figures S75 for **PH***n* and S76 for the 2-aryl-1,3,4-trifluorotriphenylenes, Table S8). They exhibit one sharp and very intense small angle diffraction peak, along, as the chain-length increases in the **PH***n* series or depending of the nature of the pending aryl in the aryl-substituted triphenylene series, additional weaker but sharp reflections, with a reciprocal d spacing in the ratio 1:√3:√4. These features, which are indicative of long-range ordered low-dimensional lattices, are most readily assigned to the (10), (11) and (20) reflections of a columnar phase with a hexagonal lattice, in agreement with POM observations. In the large-angle region, one broad scattering halo spreading between 4.2 and 4.5 Å corresponding to the overlap of undifferentiated, lateral distances between molten aliphatic tails (h_{ch}) and between aryl fragments (h_{Ar}), respectively, and a very intense and sharp signal, corresponding to the π-π intracolumnar stacking periodicity between adjacent aromatic cores (this signal decreases with temperature in the **PH***n* series); this stacking distance is comprised at ca. 3.44-3.47 and 3.54-3.66 Å at low and high temperatures, respectively for **PH***n* series, and at 3.44-3.52 and 3.56-3.58 Å for the other 2-aryl-1,3,4-trifluorotriphenylenes, respectively. The hexagonal columnar phase for all the compounds thus results from the long-range stacking of the central discotic molecular parts into column, located at the nodes of a hexagonal array; the high intensity of the signal corresponding to the stacking periodicity and the correlation length of stacking (with columnar stacks of ca. 10 to 25 molecules) suggest that, in all cases, the flat mesogenic portions stack rather parallel on top of each other in the columns with no or small tilt (Table 1). As for the pending aryl fragments, not directly involved in the stacking, they are partly blended with the aliphatic chain's continuum separating the columns (Figure 4). The variation of the columnar cross-section shows a linear

increase with chain-length, confirming that in the **PH***n* series, the mode or organization is the same throughout with no change of tilt (Table 1, Figure S77). For the other aryl-substituted triphenylenes, the cross-section is more or less in the same range, depending on the bulkiness of the aryl group, though with a slight increase in the sequence **NAA**8, **PH**8, **BT**8, **PY**8, **NAB**8 (ca. 370-390 Å^2), and is substantially increased for **TP**8 (410 Å^2) and **TPE**8 (450 Å^2), with the most voluminous aryl fragments. In the mesophase, the central flat triphenylene rings are stacked almost parallel to each other (Table 1) with a certain degree of rotational freedom with respect to the columnar axis and translational freedom with respect to the lattice plane. This is partly due to the presence of the aliphatic chains, which promotes alternation between chains and aryl groups, and to the maximization of the intermolecular arene-perfluoroarene interactions (Figure 4).[42] The protruding molten aryl groups are thus partly rejected outside of the columnar cores, and contribute to the aliphatic continuum whilst affecting at the same time the shape of aromatic-aliphatic interface i.e. diffuse interfaces.[43-45] These aryl groups also likely interact with other aryl groups between and within columns, which could explain the unexpected variation in mesophase stability (Figure 3b). Such an arrangement causes the formation of columns with an average cylindrical shape surrounded by the merging of the peripheral molten aryls and the chains into a continuum (Figure 4).[45]

Note that for the short-chain compounds, **PH**3 and **PH**4, the reduction of the aliphatic volume due to chains' shortening strongly reduces the density contrast between the rich-electron aromatic columns and the aliphatic chains, explaining the reduction of the small-angle reflections' intensity, and probably with the lowering of the temperature, to the formation of 3D or plastic crystal phase (the presence of sharp peaks in the molten chain angular range, reveal a lattice expansion in the third dimension; this phase, although insufficiently characterized, was labelled as M_{hex}).

Table 1. Geometrical and parameters of the columnar mesophases of the various 2-aryl-1,3,4-trifluorotriphenylenes.

Compds	Temp.[a]	a/A[b]	$h_\pi(\xi)/h_{ch}$[c]	V_{mol}/ρ[d]	h_{mol}[e]	ψ[f]
PH3	180	a = 16.32	3.65, h_π (87)	883	3.83	18
Col_{hex}		A = 230.6	3.62, h_{ch}	1.111		
PH4	180	a = 17.43	3.66, h_π (84)	1004	3.81	16
Col_{hex}		A = 263.3	3.63, h_{ch}	1.069		
PH6	150	a = 19.04	4.17, h_{ch}	1214	3.87	23
Col_{hex}		A = 314.0	3.57, h_π (51)	1.038		
	25	a = 18.83	4.20, h_{ch}	1119	3.64	19
		A = 307.2	3.44, h_π (85)	1.126		
PH8	120	a = 20.84	4.43, h_{ch}	1419	3.77	20
Col_{hex}		A = 376.2	3.54, h_π (48)	1.019		
	25	a = 20.61	4.34, h_{ch}	1335	3.63	19
		A = 367.7	3.44, h_π (59)	1.084		
PH10	100	a = 22.61	4.46, h_{ch}	1627	3.68	16
Col_{hex}		A = 442.6	3.54, h_π (59)	1.004		
	50	a = 22.22	4.43, h_{ch}	1575	3.68	19
		A = 427.6	3.47, h_π (68)	1.037		
PH12	80	a = 24.19	4.45, h_{ch}	1831	3.61	13
Col_{hex}		A = 506.8	3.51, h_π (50)	0.994		
	40	a = 24.16	4.34, h_{ch}	1784	3.53	11
		A = 505.3	3.46, h_π (66)	1.020		
NAA8	100	a = 20.77	4.46, h_{ch}	1432	3.83	21
Col_{hex}		A = 373.7	3.58, h_π (55)	1.068		
	50	a = 20.62	4.40, h_{ch}	1388	3.77	21
		A = 368.4	3.51, h_π (67)	1.102		
PY8	100	a = 21.00	4.24, h_{ch}	1519	3.97	26
Col_{hex}		A = 382.1	3.58, h_π (50)	1.088		
	50	a = 21.74	4.18, h_{ch}	1474	3.96	28
		A = 372.5	3.51, h_π (68)	1.121		
TPE8	80	a = 22.91	4.34, h_{ch}	1738	3.82	23
Col_{hex}		A = 454.5	3.52, h_π (53)	1.075		

	40	a = 22.79 A = 449.7	4.27, h_{ch} 3.47, h_{π} (63)	1705 1.096	3.79	24
BT8 Col_{hex}	160	a = 20.89 A = 377.9	4.44, h_{ch} 3.56, h_{π} (40)	1487 1.036	3.94	26
	100	a = 20.67 A = 370.0	4.42, h_{ch} 3.50, h_{π} (54)	1423 1.082	3.85	25
	40	a = 20.45 A = 362.2	4.35, h_{ch} 3.44, h_{π} (59)	1371 1.123	3.78	24
NAB8 Col_{hex}	150	a = 21.20 A = 389.4	4.42, h_{ch} 3.57, h_{π} (54)	1507 1.015	3.87	23
	100	a = 21.11 A = 386.0	4.37, h_{ch} 3.51, h_{π} (72)	1455 1.051	3.77	21
	40	a = 21.07 A = 384.4	4.33, h_{ch} 3.44, h_{π} (78)	1403 1.090	3.65	19
TP8 Col_{hex}	140	a = 22.09 A = 422.6	4.37, h_{ch} 3.56, h_{π} (64)	1582 1.072	3.74	18
	90	a = 21.90 A = 415.3	4.34, h_{ch} 3.51, h_{π} (73)	1531 1.108	3.69	18
	40	a = 21.70 A = 407.9	4.27, h_{ch} 3.45, h_{π} (80)	1489 1.139	3.65	19

[a]Temperature of experiment (°C); [b]Lattice parameter, a (Å) and area, $A = a^2\sqrt{3}/2$ (Å^2); [c]Average face-to-face stacking distance between consecutive mesogens, h_{π} (Å), determined from scattering maximum from SWAXS pattern, and ξ, correlation length (Å) calculated by Debye-Scherrer formula; h_{ch}, average distance between molten chains; [d]Molecular volume (Å^3) and density (g cm^{-3}) calculated from partial volumes of reference substances: $V_{mol} = V_{ar} + V_{ch}$, the sum of the volume of the aromatic part, V_{ar} (from reference compounds) and the volume of the chains, V_{ch};[46] $\rho = MW/(N_A.V_{mol})$; [e]Columnar slice thickness, $h_{mol} = V_{mol}/A$ (Å); [f]Out-of-plane tilt angle of mesogen cores inside columns (°), $\psi = \arccos(h_{\pi}/h_{mol})$.

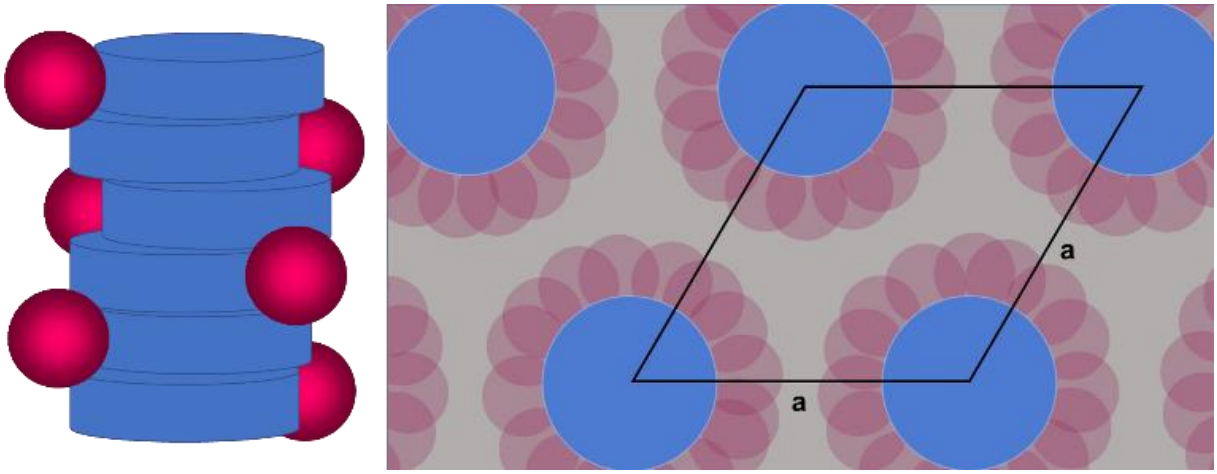

Figure 4. Schematic representation (side and top views) of one triphenylene column with pending aryl moieties, and of the self-assembly of the 2-aryl-1,3,4-trifluorotriphenylenes in supramolecular columns and their arrangement within the hexagonal lattice of parameter a (blue: triphenylene disc; red: aryl pending groups; grey: aliphatic continuum).

UV-Vis. Absorption and fluoresecent emission

Fluorescent and light-emitting large, π-conjugated DLCs still attract the interest of scientists not only for academic reasons but also for their potential applications and uses in OLED, biological probes, chemical sensors, stimuli responses and circularly polarized light-emitting materials.[47-54] Large aromatic systems containing pyrene (**PY**8) and tetraphenylethene (**TPE**8) are particularly important as potential fluorescent and aggregate-induced light-emitting functional materials, respectively.[55]

The UV-Vis absorption and fluorescent emission of the synthesized molecules were studied in both dilute solutions and in thin films (emission) to understand the effects of the π-conjugation extension, intermolecular

interactions and coplanarity on the optical properties. All the molecules have their strongest absorption peak around 300 nm, and weaker ones between 325 to 400 nm, whose position maxima depend on the aryl substituent (Figure 5a). The latter absorption peaks correspond to the intramolecular charge transfer (ICT) between the HOMO-LUMO frontier molecular orbitals. The emission spectra in solution display one single broad peak (Figure 5b), with an emission peak maximum spanning from 402 to 463 nm, reflecting the π-conjugation extension between triphenylene core and the side aryl substituents. They emit at different wavelength, increasing from **PH**8 and **NAA**8, that emit at ca. 402 nm, followed by **NAB**8 (416 nm), **TPE**8 (426 nm) and **TP**8 (431 nm), and then at larger wavelengths by **BT**8 (454 nm) and **PY**8 (463 nm). In the solid state, emission again display only one single, broad peak (450-700 nm), at larger wavelengths than in solution, this redshift being caused by molecular aggregation (Figure 5c). The order is changed from solution, and **TPE**8 film emits at 565 nm, reflecting its feature for aggregation-induced emission (AIE).[55] The fluorescence absolute quantum yields were measured in dilute solution, and **PY**8 shows the highest Φ value of 57%; the other molecules display Φ values between 22 to 26%. **PY**8 and **TPE**8 have potential uses as mesogenic light-emitting materials (Table 2).

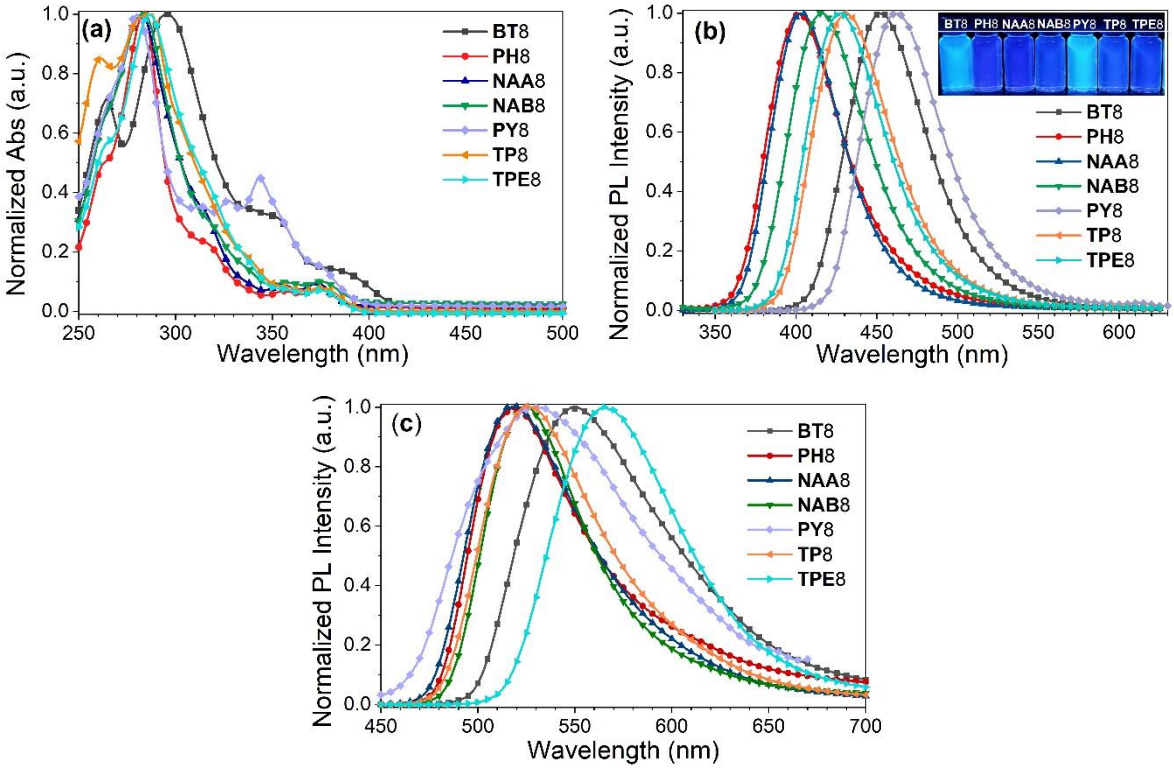

Figure 5. (a) UV/Vis. absorption and (b) fluorescent spectra in THF micromolar solution, and (c) emission in solid thin-films of the various 2-aryl-1,3,4-trifluorotriphenylenes.

Table 2. UV-Vis and photoluminescence of the 2-aryl-1,3,4-trifluorotriphenylenes.

Compd.	$\lambda_{abs}{}^{a}$	ε^{b}	λ_{em} (QY)^{c}	$\lambda_{em}{}^{d}$
BT8	296 351 382	5.54	454 (21)	550
PH8	284 356 374	1.39	402 (22)	518
NAA8	283 353 375	1.82	402 (22)	519
NAB8	283 356 375	1.83	416 (22)	526
PY8	280 328 344	9.99	463 (57)	527
TP8	287 376	1.78	431 (24)	525
TPE8	287 376	1.24	426 (26)	565

[a]Absorption wavelength (nm); [b]Molar absorption efficiency (×10^4, L mol^{-1} cm^{-1}); [c]Solution emission wavelength (nm) and absolute quantum yield (%); [d]Thin-solid film emission (nm). The absorption spectra were measured in THF concentration of 10^{-5} mol/L; the fluorescent emission spectra were measured in THF with concentration of 10^{-6} mol/L.

DFT computation results

The electronic structures of the methoxy homologs of the synthesized fluorinated arenes were studied by theoretical calculation of DFT, using method of B3LYP-D3 with 6-311++g(d,p) set. The molecular conformations with minimized energy, their HOMO and LUMO, energy gaps, are summarized in Figures 6 and S78. Both in gas state and in THF diluted solution, these aryl-substituted molecules present intramolecular electron transfer (ICT), from the electron-rich moiety with tetraalkoxy-substitution to the other trifluorobenzene-Ar part. The calculated results of HOMO-LUMO energy gaps agree very well with the experimental results of fluorescence: **BT**1, **PY**1 and **TPE**1 have narrowed energy band gaps, and emit lights at longer wavelength.

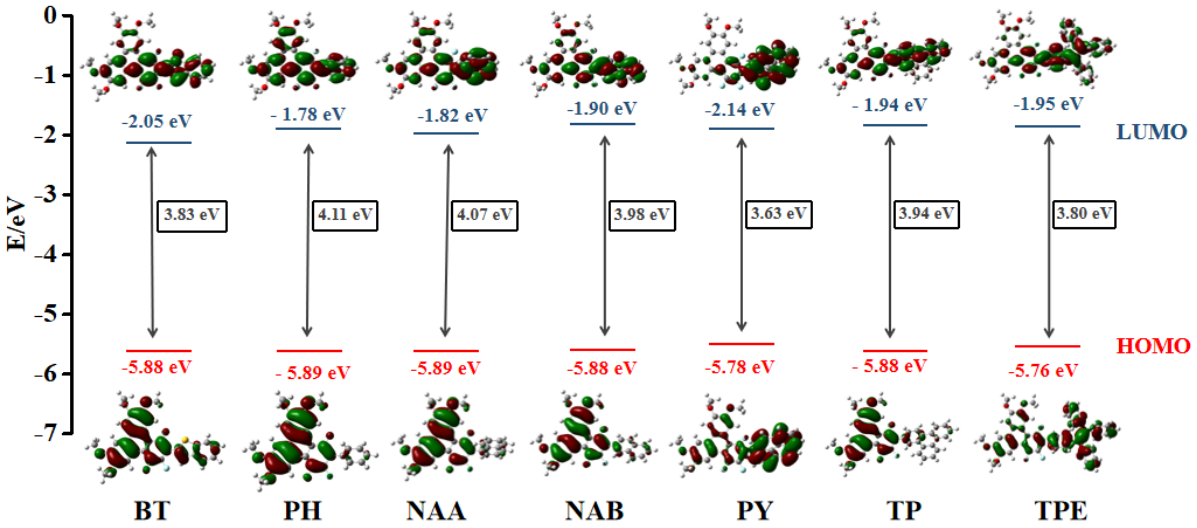

Figure 6. HOMO-LUMO and energy gap of the methoxy derivatives of the 2-aryl-1,3,4-trifluorotriphenylenes in THF.

Charge carrier mobility by time-of-flight (TOF) technique

π-Conjugated discotic liquid crystalline materials usually tend to self-organize into ordered supramolecular structures, via the stacking into columnar mesophases through strong π-π interactions between the poly-aromatic cores. They thus have attracted considerable attention as emerging promising one-dimensional semiconducting soft materials able to form easily solution processible and homogeneous, self-healing films, essential features for the improvement of charge-transport properties in device performance, and potential applications in laser jet printers as photoconductors and organic field effect transistors as semiconductors.[8,9,12,56] Electron-rich DLCs usually transport hole as p-type semiconductors, and electron-deficient DLCs transport electron as n-type semiconductors. The fluorinated p-type can be n-type or ambipolar semiconductors as fluorine atoms on arene can effectively adjust the electron density of the polycylic aromatic rings.

Photocurrent of time-of-flight technique is a widely used method to measure the charge carrier mobility value of bulk liquid crystalline samples. Usually the ITO coated sample cell thickness for TOF measurement is in the range of 10-20 μm, which is very similar to that of printed electronic devices. Further, TOF results are direct, precise and reliable, and both positive (hole) and negative (electron) charge carrier can be measured directly. These advantage features of the TOF technique make it applied widely for semiconducting property studies for DLC samples.

PY8 was chosen for this measurement due to its moderate clearing temperature of 117°C, and to its large pyrene core. The sample was filled in the cell by capillary force above the clearing temperature and the sample was homeotropically aligned between two electrodes and the supplied supramolecular columns used as the charge hopping pathway. The photoconductivity results are summarized in Figure 7 and SI.

The transient photocurrent decay curves are non-dispersive, the drift time can be readout accurately (Figure 7b-d). **PY**8 displays positive charge conductivity even in the isotropic liquid state (4 x 10^{-5} cm^2 V^{-1} s^{-1}, Figure 7a), possibly because of the high ratio of aromatic core/alkyl side chain. In the Col_{hex} phase at 100 °C, the value jumps to 10^{-3} cm^2 V^{-1} s^{-1}, about 25 time higher than that of the isotropic state, demonstrating the anisotropic charge mobility feature of columnar mesophase (Figure 7a). Then on cooling, down to 30 °C, the mobility rate decreases to 4 x 10^{-4} cm^2 V^{-1} s^{-1}, showing the small temperature dependence character of the photoconductivity (Figure 7a). The measured TOF values are almost non-dependent on the applied electric field (Figure 7b-d).

Thus, TOF photoconductivity values for **PY**8, in the range of 10^{-3} cm^2 V^{-1} s^{-1}, are higher than for the archetypical 2,3,6,7,10,11-hexakis(octyloxy)triphenylene, displaying hole mobility rate of 10^{-4} cm^2 V^{-1} s^{-1}.[57] This high mobility value may result from to the higher intracolumnar order triggered by stronger arene-perfluoroarene interactions that stabilize regular long-range molecular stacking.

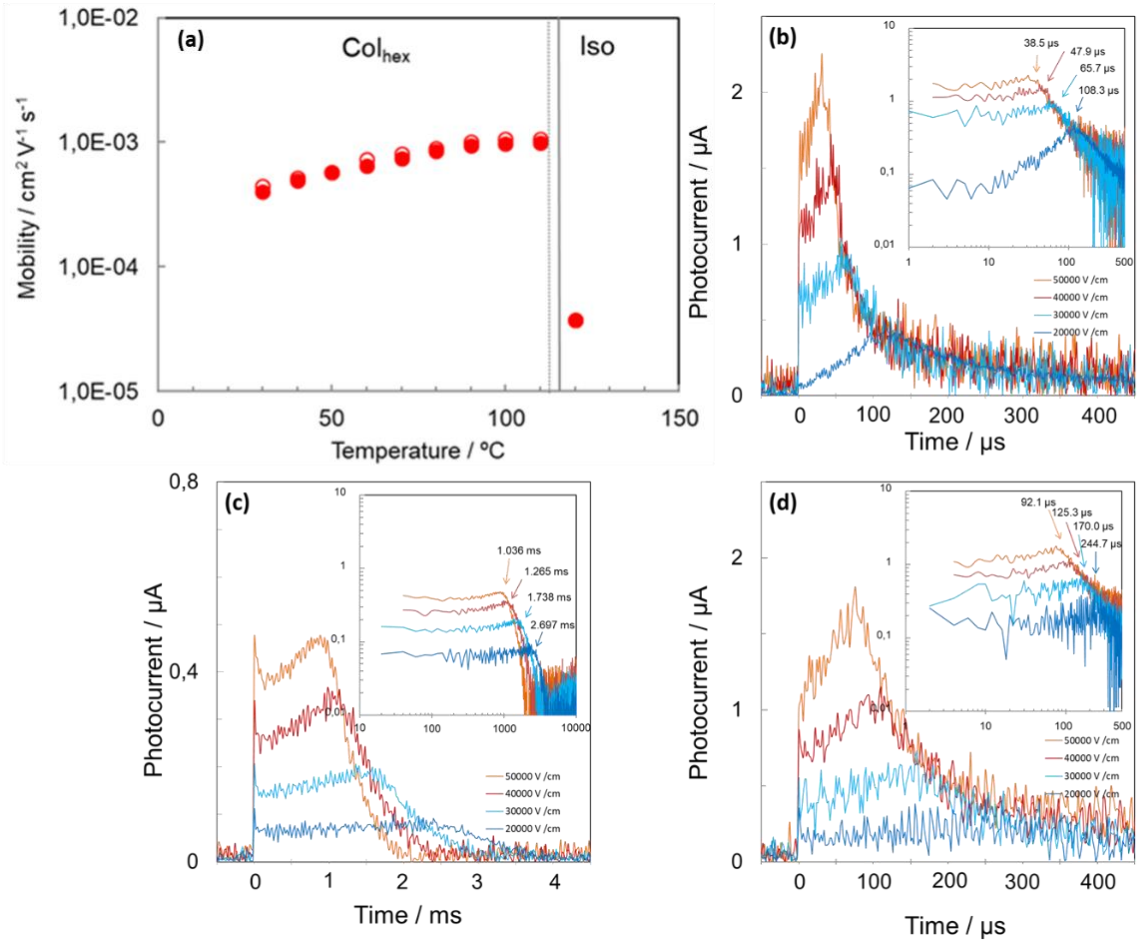

Figure 7. Photoconductivity of **PY**8 measured by transient photocurrent TOF technique (cell thickness: 19.6 µm): (a) Temperature-dependent of hole mobility µ values measured on both on heating (○) and cooling (●). (b-d) Electric field dependency of positive photocurrent decay curves (normal plot and inserted log-log plot): (a) in Col_{hex} phase at 100 °C; (b) in the isotropic liquid state at 120 °C; (c) in Col_{hex} phase at 30 °C (on cooling).

Conclusions

Two series of fluorine-containing discotic liquid crystals have been synthesized by arene fluorine nucleophilic substitution reaction, S_NFar, without the use of transition metal catalyst. In particular, the synthetic combination of low symmetry fluoro-triphenylene discotic columnar mesogens with potentially interesting AIE functional groups such as tetraphenylethene and pyrene is presented here for the first time.

All the compounds, irrespective of the alkyl chain-lengths or the aryl-substitution, show a broad temperature-range Col_{hex} mesophase with high thermal stability, attributed to efficient face-to-face π-stacking driven

concomitantly by the establishment of long-range non-covalent perfluoroarene-arene, π-π intermolecular interactions and self-segregation between alkyl chain and aromatic core. Most of them are liquid crystalline at room temperature. These compounds also exhibit blue light fluorescence, the emission of **TPE**8 being shifted to 565 nm and **PY**8 showing a high fluorescent quantum yield of 57%. Further, the transient photocurrent time-of-flight technique measured hole mobility for **PY**8 in the range of 10^{-3} cm^2 V^{-1} s^{-1}, larger than for the archetypical 2,3,6,7,10,11-hexa(octyloxy)triphenelyenes.

The fluorine-substitution of aromatic core results in potentially strong dipolar DLCs and this strategy is being increasingly developed for numerous applications. The facile synthesis of such a variety of highly functional, low-symmetry triphenylene derivatives, endowed with excellent self-assembly, optical and electronic properties, proposed here, is obviously not limited to these simple molecular skeletons and could be extended to a wide range of novel multifunctional molecular materials with more complex molecular structures of interest in the fields of organic electronics and displays.

Author Contributions

Conceptualization, K.-Q.Z.; methodology, K.-Q.Z.; formal analysis, H.-M.P., J.H., W.-H.Y., K.-Q.Z. and B.D.; investigation, H.-M.P., J.H., W.-H.Y., K.-Q.Z., H.M. and B.D.; data curation, K.-Q.Z., H.M. and B.D.; writing—original draft preparation, K.-Q.Z. and B.D.; writing—review and editing, K.-Q.Z. and B.D.; supervision, K.-Q.Z.; funding acquisition, K.-Q.Z., P.H., and B.-Q.W. All authors have read and agreed to the published version of the manuscript.

Conflicts of interest

There are no conflicts to declare.

Acknowledgements

We thank the National Natural Science Foundation of China for funding (51773140, 51973143). BD thanks the CNRS and the University of Strasbourg for constant support. Dr Hirosato Monobe, from Nanomaterials Research Institute, Department of Materials and Chemistry, National Institute of Advanced Industrial Science and Technology (AIST), Kansai, Ikeda, Osaka 563-8577, Japan, is thanked for the TOF measurements.

Notes and references

1 T. Wöhrle, I. Wurzbach, J. Kirres, A. Kostidou, N. Kapernaum, J. Litterscheidt, J. C. Haenle, P. Staffeld, A. Baro, F. Giesselmann and S. Laschat, *Chem. Rev.*, 2016, **116**, 1139-1241.
2 S. Sergeyev, W. Pisula and Y. H. Geerts, *Chem. Soc. Rev*., 2007, **36**, 1902-1929.
3 T. Kato, M. Yoshio, T. Ichikawa, B. Soberats, H. Ohno and M. Funahashi, *Nat. Rev. Mater*., 2017, **2**, 17001.
4 J. Wu, W. Pisula and K. Müllen, *Chem. Rev*., 2007, **107**, 718-747.
5 X. Feng, W. Pisula and K. Müllen, *Pure Appl. Chem*., 2009, **81**, 2203-2224.
6 M. O'Neill and S. M. Kelly, *Adv. Mater*., 2011, **23**, 566-584.
7 R. J. Bushby and K. Kawata, *Liq. Cryst*., 2011, **38**, 1415-1426.
8 Y Shimizu, K Oikawa, K Nakayama and D Guillon, *J. Mater. Chem*., 2007, **17**, 4223-4229.
9 R. Termine and A. Golemme, *Int. J. Mol. Sci*., 2021, **22**, 877.
10 K. Q. Zhao, C. Chen, H. Monobe, P. Hu, B. Q. Wang and Y. Shimizu, *Chem. Commun*., 2011, **47**, 6290-6292.
11 K.-Q. Zhao, L.-L. An, X.-B. Zhang, W.-H. Yu, P. Hu, B.-Q. Wang, J. Xu, Q.-D. Zeng, H. Monobe, Y. Shimizu, B. Heinrich and B. Donnio, *Chem. Eur. J*., 2015, **21**, 10379-10390.
12 R. De and S. K. Pal, *Chem. Commun*., 2023, **59**, 3050-3066.
13 M. Jasiński, J. Szczytko, D. Pociecha, H. Monobe and P. Kaszyński, *J. Am. Chem. Soc*., 2016, **138**, 9421-9424.
14 W.-J. Deng, S. Liu, H. Lin, K.-X. Zhao, X.-Y. Bai, K.-Q. Zhao, P. Hu, B.-Q. Wang, H. Monobe and Bertrand Donnio, *New J. Chem*., 2022, **46**, 7936-7949.
15 Q. Zeng, S. Liu, H. Lin, K.-X. Zhao, X.-Y. Bai, K.-Q. Zhao, P. Hu, B.-Q. Wang and B. Donnio, *Molecules*, 2023, **28**, 1721.
16 J.-F. Hang, H. Lin, K.-Q. Zhao, P. Hu, B.-Q. Wang, H. Monobe, C. Zhu and B. Donnio, *Eur. J. Org. Chem*., 2021, **2021**, 1989-2002.
17 T. Ma, Y.-J. Zhong, H.-F. Wang, K.-Q. Zhao, B.-Q. Wang, P. Hu, H. Monobe and B. Donnio, *Chem. Asian J*., 2021, **16**, 1106-1117.
18 H. Lin, K.-X. Zhao, M. Jing, X.-H. Long, K.-Q. Zhao, P. Hu, B.-Q. Wang, P. Lei, Q.-D. Zeng and B. Donnio, *J. Mater. Chem. C*, 2022, **10**, 14453-14470.

19 K.-C. Zhao, J.-Q. Du, H.-F. Wang, K.-Q. Zhao, P. Hu, B.-Q. Wang, H. Monobe, B. Heinrich and B. Donnio, *Chem. Asian J.*, 2019, **14**, 462-470.
20 N. Boden, R. C. Borner, R. J. Bushby, A. N. Cammidge and M. V. Jesudason, *Liq. Cryst.*, 1993, **15**, 851-858.
21 S. Kumar, *Liq. Cryst.*, 2004, **31**, 1037-1059.
22 D. Perez and E. Guitian, *Chem. Soc. Rev.*, 2004, 33, 274-283.
23 A. O. Sarham and C. Bolm, *Chem. Soc. Rev.*, 2009, **38**, 2730-2744.
24 Z. W. Schroeder, J. LeDrew, V. M. Selmani and K. E. Maly, *RSC Adv.*, 2021, **11**, 39564-39569.
25 M. Hird, *Chem. Soc. Rev.*, 2007, *36*, 2070-2095.
26 D. M. Cho, S. R. Parkin and M. D. Watson, *Org. Lett.*, 2005, **7**, 1067-1068.
27 Z. Wang, C. Wang and Z. Xi, *Tet. Lett.*, 2006, **47**, 4157-4160.
28 H. Zhang, J. Han, X. Jin and P. Duan, *Angew. Chem. Int. Ed. Engl.*, 2021, **60**, 4575-4580.
29 Z. Li, M. Powers, K. Ivey, S. Adas, B. Ellman, S. D. Bunge and R. J. Twieg, *Mater. Adv.*, 2022, **3**, 534–546.
30 R. E. Yardley, J. A. Paquette, H. Taing, H. M. Gaebler, S. Holger Eichhorn, I. P. Hamilton and K. E. Maly, *Org. Lett.*, 2019, **21**, 10102-10105.
31 N. Boden, R. J. Bushby, A. N. Cammidge, S. Duckworth and G. Headdock, *J. Mater. Chem.*, 1997, **7**, 601-605.
32 K.-Q. Zhao, Min Jing, L.-L. An, J.-Q. Du, Y.-H. Wang, P. Hu, B.-Q. Wang, H. Monobe, B. Heinrich and B. Donnio, *J. Mater. Chem. C*, 2017, **5**, 669-682.
33 K.-Q. Zhao, Y. Gao, W.-H. Yu, P. Hu, B.-Q. Wang, B. Heinrich and B. Donnio, *Eur. J. Org. Chem.*, 2016, **2016**, 2802-2814.
34 K.-Q. Zhao, J.-Q. Du, X.-H. Long, M. Jing, B.-Q. Wang, P. Hu, H. Monobe, B. Henrich and B. Donnio, *Dyes Pig.*, 2017, **143**, 252-260.
35 V. G. Farias, W. C. Costa, J. Eccher, I. H. Bechtold, F. Durola and H. Bock, *Chem. Eur. J.*, 2021, **27**, 9003-9010.
36 Y. Sasada, H. Monobe, Y. Ueda and Y. Shimizu, *Chem. Lett.*, 2007, **36**, 584-585.
37 Y. Sasada, H. Monobe, Y. Ueda and Y. Shimizu, *Chem. Commun.*, 2008, 1452-1454.
38 (a) C. Tschierske, *Top. Curr. Chem.*, 2012, **318**, 1-108. (b) K. Kishikawa, *Isr. J. Chem.*, 2012, **52**, 800–808.
39 (a) M. Weck, A. R. Dunn, K. Matsumoto, G. W. Coates, E. B. Lobkovsky and R. H. Grubbs, *Angew. Chem. Int. Ed.*, 1999, **38**, 2741-2745. (b) K. Kishikawa, K. Oda, S. Aikyo and S. Kohmoto, *Angew. Chem. Int. Ed.*, 2007, **46**, 764-768.
40 M.-M. Zhou, J. He, H.-M. Pan, Q. Zeng, H. Lin, K.-Q. Zhao, P. Hu, B.-Q. Wang, B. Donnio, *Chem. Eur. J.*, 2023, in press http://dx.doi.org/10.1002/chem.202301829
41 (a) J. L. Schulte and S. Laschat, *Synthesis*, 1999, **3**, 475–478. (b) N Boden, R J Bushby, Z Lu and G Headdock, *Tet. Lett.*, 2000, **41**, 10117-10120.
42 M. Powers, R. J. Twieg, J. Portman and B. Ellman, *J. Chem. Phys.*, 2022, *157*, 134901
43 S. Coco, C. Cordovilla, C. Domínguez, B. Donnio, P. Espinet and D. Guillon, *Chem. Mater.*, 2009, **21**, 3282-3289.
44 C. Dominguez, B. Heinrich, B. Donnio, S. Coco and P. Espinet, *Chem. Eur. J.*, 2013, **19**, 5988-5995.
45 A. B. Miguel-Coello, M. Bardaji, S. Coco, B. Donnio, B. Heinrich and P. Espinet, *Inorg. Chem.*, 2014, **53**, 10893-10902.
46 B. Donnio, B. Heinrich, H. Allouchi, J. Kain, S. Dele, D. Guillon and D. W. Bruce, *J. Am. Chem. Soc.*, 2004, **126**, 15258–15268.
47 H. Yu and G. H. Mehl, *Liq. Cryst.*, 2021, **48**, 1750-1757.
48 R. R. Parker, D. Liu, X. Yu, A. C. Whitwood, W. Zhu, J. A. G. Williams, Y. Wang, J. M. Lynam and D. W. Bruce, *J. Mater. Chem. C*, 2021, **9**, 1287-1302.
49 Z. Yu, X. M. Chen, Z. Y. Liu, M. Wang, S. Huang and H. Yang, *Chem. Commun.*, 2021, **57**, 911-914.
50 Y. Li, A. Concellón, C.-J. Lin, N. A. Romero, S. Lin, T. M. Swager, *Chem. Sci.*, 2020, **11**, 4695-4701.
51 M. Barcenilla, M. J. Baena, B. Donnio, B. Heinrich, L. Gutiérrez, S. Coco and P. Espinet, *J. Mater. Chem. C*, 2022, **10**, 9222-9231.
52 J. Dai, K.-Q. Zhao, B.-Q. Wang, P. Hu, B. Heinrich and B. Donnio, *J. Mater. Chem. C*, 2020, **8**, 4215-4225.
53 B. Mu, T. Ma, Z. Zhang, X. Hao, L. Wang, J. Wang, H.Yan, W. Tian, *Chem. Eur. J.*, 2023, **29**, e202300320.
54 M. La Deda, G. Di Maio, A. Candreva, B. Heinrich, A.-A. Andelescu, E. Popa, E. Voirin, V. Badea, M. Amati, O. Costişor, B. Donnio and E. I. Szerb, *J. Mater. Chem. C*, 2022, **10**, 115-125.
55 J. Mei, N. L. C. Leung, R. T. K. Kwok, J. W. Y. Lam and B. Z. Tang, *Chem. Rev.*, 2015, **115**, 11718-11940.
56 V. Bhat S. M. Vadivel, D. P. Singh, V. A. Raghunathan, A. Roy and S. Kumar, *Chem. Eur. J.*, 2023, **29**, e202300227.
57 H. Monobe, Y. Shimizu, S. Okamoto and H. Enomoto, *Mol. Cryst. Liq. Cryst.*, 2007, **476**, 31/[277]-41/[287].